*Article*

# Effect of Cu₂Te Back Surface Interfacial Layer on Cadmium Telluride Thin Film Solar Cell Performance from Numerical Analysis

Muhammad Najib Harif [1,2,*], Camellia Doroody [1,3,*], Allina Nadzri [2], Hasrul Nisham Rosly [1,4], Nur Irwany Ahmad [1,5], Mustapha Isah [1,6] and Nowshad Amin [1,3]

1 College of Engineering, Universiti Tenaga Nasional (@The Energy University), Jalan Ikram-UNITEN, Kajang 43000, Selangor, Malaysia
2 Faculty of Applied Sciences, Universiti Teknologi MARA, Cawangan Negeri Sembilan, Kuala Pilah 72000, Malaysia
3 Institute of Sustainable Energy, Universiti Tenaga Nasional (@The Energy University), Jalan Ikram-UNITEN, Kajang 43000, Selangor, Malaysia
4 Faculty of Electrical and Electronic Engineering Technology, Universiti Teknikal Malaysia Melaka, Durian Tunggal, Melaka 76100, Malaysia
5 Faculty of Electrical Engineering & Technology, Universiti Malaysia Perlis (UniMAP), Kangar 02600, Perlis, Malaysia
6 Department of Physics, Kaduna State University, P.M.B, 2339, Kaduna 800283, Nigeria
* Correspondence: najib@uitm.edu.my (M.N.H.); camellia@uniten.edu.my (C.D.)

**Abstract:** Even though substantial advances made in the device configuration of the frontal layers of the superstrate cadmium telluride (CdTe) solar cell device have contributed to conversion efficiency, unresolved challenges remain in regard to controlling the self-compensation and minority carrier recombination at the back contact that limits the efficiency. In this study, a SCAPS-1D simulator was used to analyze the loss mechanism and performance limitations due to the band-bending effect upon copper chloride treatment and subsequent Cu₂Te layer formation as the back contact buffer layer. The optimal energy bandgap range for the proposed back surface layer of Cu₂Te is derived to be in the range of 1.1 eV to 1.3 eV for the maximum conversion efficiency, i.e., around 21.3%. Moreover, the impacts of absorber layer's carrier concentration with respect to CdTe film thickness, bandgap, and operational temperature are analyzed. The optimized design reveals that the acceptor concentration contributes significantly to the performance of the CdTe devices, including spectral response. Consequently, the optimized thickness of the CdTe absorber layer with a Cu-based back contact is found to be 2.5 μm. Moreover, the effect of temperature ranging from 30 °C to 100 °C as the operating condition of the CdTe thin-film solar cells is addressed, which demonstrates an increasing recombination tread once the device temperature exceeds 60 °C, thus affecting the stability of the solar cells.

**Keywords:** energy; solar photovoltaic cells; cadmium telluride; thin film; SCAPS; doping concentration

## 1. Introduction

In the last decade, the efficiency of cadmium telluride (CdTe) solar cells has grown from 16.7% to 22.1% [1]. Given that CdTe grains are 1000 times smaller than silicon grains, the CdTe device performance is substantially greater than ideal polycrystalline gallium arsenide cells at 18.4% and close to the record for multi-crystalline silicon cells, at 22.3% [2]. In recent years, various types of CdTe nanoparticles were prepared through organometallic routes [3–5]. Despite CdTe's rapid growth rate and high defect density, the addition of chlorine to CdTe has contributed to the superior CdTe device performance [6]. The chlorine inclusion typically enhanced doping potential, carrier lifetime, and mobility within CdTe grains, grain boundaries, and at the absorber's frontal interface [7]. However,

there are no reports on the reduction in recombination at grain boundaries using $CdCl_2$ [8]. Copper (Cu) inclusion, on the other hand, has been recognized as the most effective dopant for increasing hole concentration and improving ohmic contact in superstrate CdTe thin films [9]. Recent studies on the $CuCl_2$ treatment using optimum Cu concentration indicated a reduction in deep defects, trap state levels, and recombination velocity, which was reduced by some orders of magnitude due to the high permeability of Cu ions at grain boundaries [10]. Moreover, many other p-type alternatives, such as Te, $Sb_xTe$, $Mo_xO$, $Ti_xSe$, $Cu_9S_5$, etc. [11–13], have been used to form ohmic contacts that also improved the contact electrodes; however, such buffer layers could not be stable and optimal as much as long-established Cu inclusive layers, due to their different shortcomings [14]. Metal oxides, for example, have a high work function but poor electrical conductivity, and inefficient Cu ions cause impaired stability using some of the specified buffers. Accordingly, $CuCl_2$ is demonstrated as a beneficial treatment in the optimization of the back contact performance by removing the oxides and forming a tellurium-rich p+ $Cu_2Te$ layer [15]. Indirectly doped narrow-gap $Cu_2Te$ has a low resistance, relatively high mobility, and hole concentration. Experiments on the fabrication of a $CdTe/Cu_2Te$ heterostructure highlighted the formation of a short band offset at the $CdTe/Cu_2Te$ junction, making $Cu_2Cl$ a practical and beneficial doping and treatment strategy for improving the efficiency of CdTe thin films [16,17]. Full device performance was also reported with up to 19% efficiency after $Cu_2Cl$ treatment, resulting from the reduced recombination rate at the CdTe bulk and front, as well as the rear interface [18]. In addition, while multiple possible interactions can occur simultaneously and increase the complexity of the analysis at the experimental scale, it is essential to develop the proposed thin film layouts and study the particular response where at least part of the mechanisms can be maintained as constant [19]. Simulation or numerical modeling as an imperative tool enables designing and analyzing the performance of the solar cells, particularly thin-film solar cells. It eliminates the prototypes' production cost by enabling all parameters to be modified in the modeling scale [20]. There have been reports of utilizing PC1D, DFT, wxAMPS, MATLAB, AFORS-HET, SILVACO, and Solar Cell Capacitance Simulator (SCAPS 1D) to model Cu integration in CdTe thin film devices [21–23]. The suggested thin films' electron properties cannot be accurately estimated by any of the aforementioned tools; thus, SCAPS-1D is employed, with a focus on the importance of the back surface field (BSF) [24]. SCAPS-1D originally created at the University of Ghent for detailed numerical and analytical modeling of thin film technology, primarily for CdTe and CIGS thin-film solar cells [25]. The recent findings employing SCAPS to investigate the effect of Cu doping on the performance of CdTe thin films verify the model outputs' compliance with empirically obtained results [26,27]. Moreover, the initial Fermi level offset (IFLO) concept has newly been raised by comprehensive analysis using SCAPS, which may assist doping levels in CdTe and the back contact material to be fully addressed rather than simply utilizing the valance band offset (VBO) [28]. The key advantage of adopting SCAPS-1D is the ability to analyze the characteristics of solar cells by using an existing database. It also generates data based on the operating temperature and displays recombination profiles. SCAPS-1D calculates the steady-state energy band, recombination pattern, and carrier transport, using the Poisson and hole–electron continuity equations [29]. The Shockley–Read–Hall (SRH) model is used to determine recombination currents for bulk defects. Thereby, in this study, SCAPS modeling is carried out with the primary focus on the $CuCl_2$ doping function and formation of $Cu_2Te$ in accordance with the IFLO concept. Ultimately, the maximum possible yield of the final proposed device, as well as the impact of layer-based constraints, is presented.

## 2. Methodology

SCAPS modeling is used here to analyze the charge-carrier transport and the effects of doping effect on electrical output parameters of the CdTe thin-film solar cell. Following the latest available literature on the most efficient CdTe solar cell with explicit fabrication instructions [30], the CdTe thin-film structure is proposed. To account for the possible

recombination at the Magnesium-doped zinc oxide (MZO)/CdTe interface, reasonable neutral interface defects are defined and the Shockley–Read–Hall (SRH) model is used to calculate recombination currents for bulk defects. Moreover, a fluorine-doped tin oxide (FTO) transparent conductive layer serves as the front contact in the proposed configuration, and silver (Ag) with a work function of 4.6 eV is inserted to complete the proposed thin-film structure as the device's output terminal. The complete information of the entire parameters exploited in this simulation is presented in Table 1.

**Table 1.** Materials parameter used in SCAPS simulation.

| Parameters | Layer | | | |
|---|---|---|---|---|
| | FTO [31] | MZO [32] | CdTe [33] | Te:Cu [34,35] |
| Thickness, W (nm) | 300 | 100 | (500–5000) | 2 |
| Bandgap, $E_g$ (eV) | 3.5 | 3.6 | 1.4–1.5 | 1.1 |
| Electron affinity (eV) | 4.1 | 4.5 | 4.28 | 4.2 |
| Dielectric Permittivity ($e/e_0$) | 10 | 10 | 9.4 | 10 |
| CB effective density of states (cm$^{-3}$) | $2.2 \times 10^{17}$ | $2.2 \times 10^{17}$ | $8.0 \times 10^{18}$ | $8.0 \times 10^{18}$ |
| VB effective density of states (cm$^{-3}$) | $1.8 \times 10^{18}$ | $1.8 \times 10^{18}$ | $1.8 \times 10^{19}$ | $1.8 \times 10^{19}$ |
| Electron thermal velocity (cm/s) | $1.0 \times 10^7$ | $1.0 \times 10^7$ | $1.0 \times 10^7$ | $1.0 \times 10^7$ |
| Hole thermal velocity (cm/s) | $1.0 \times 10^7$ | $1.0 \times 10^7$ | $1.0 \times 10^7$ | $1.0 \times 10^7$ |
| Electron mobility, $\mu N$ (cm$^2$/Vs) | $1.0 \times 10^2$ | $1.0 \times 10^2$ | $5.0 \times 10^2$ | $1.5 \times 10$ |
| Hole mobility, $\mu P$ (cm$^2$/Vs) | 75 | 25 | 60 | 10 |
| Shallow donor density $N_D$ (cm$^{-3}$) | $1.0 \times 10^{21}$ | $1.0 \times 10^{18}$ | $1.0 \times 10^7$ | $1.0 \times 10^7$ |
| Shallow acceptor density $N_A$ (cm$^{-3}$) | $1.0 \times 10^7$ | $1.0 \times 10^7$ | ($1.0 \times 10^{13}$ to $1.0 \times 10^{16}$) | $1.0 \times 10^{16}$ |
| Defect type | - | Acceptor | Neutral | - |
| Defect density (cm$^{-3}$) | 0.6 | 0.6 | 0.6 | 0.6 |

The CdTe superstrate device structure consists of an n-MZO/p-CdTe heterojunction with an n-type and p-type doping concentration of $1 \times 10^{18}$ cm$^{-3}$ and $2 \times 10^{14}$ cm$^{-3}$, respectively, as schematized in Figure 1a. For the CdTe absorber layer, the thickness was varied between 0.5 μm and 5.0 μm; meanwhile, the bandgap of CdTe layer varied from 1.4 eV to 1.5 eV, corresponding to the acceptor-carrier concentration. The thicknesses for the FTO layer and MZO layer were maintained at 300 nm and 100 nm, respectively, for all cases, in accord with the previous studies [30]. Furthermore, the donor density, $N_D$, was fixed at $1.0 \times 10^{18}$ cm$^{-3}$, while the acceptor density, $N_A$, ranged from $1.0 \times 10^{13}$ cm$^{-3}$ to $1.0 \times 10^{18}$ cm$^{-3}$ following the changes in doping concentration.

The SCAPS software interface is shown in Figure 1b. The dashboard panel consists of a sequence of operations. A basic thin-film-solar-cells model by default was used to obtain the temperature dependence of the effective charge density of states and thermal velocity. However, bandgap settings and electron mobility parameters are temperature independent. During the simulation, the modeled device was illuminated with an AM1.5 incident irradiance of 1000 W/m$^2$ in a room-temperature environment. In addition, to ensure the accuracy of the outputs, the optical or absorption data recorded in the experimental literature utilizing UV–Vis (Lambda-1050), (PerkinElmer, Waltham, MA, USA), were employed, and only electrical aspects were analyzed in the present modeling [36,37]. Figure 2 depicts the intrinsic energy band of the included thin films. The band offset arrows are shown to specify the carrier movements in both valence bands (VBs) and conduction bands (CBs). Similarly, as coupled with the CdTe layer, the positive initial Fermi level offset

(IFLO) displays a lower Fermi level, and the negative IFLO represents a higher Fermi level. The placements of the CB and VB at the frontal layers are estimated to be ideal with a 0.3 eV barrier height [38].
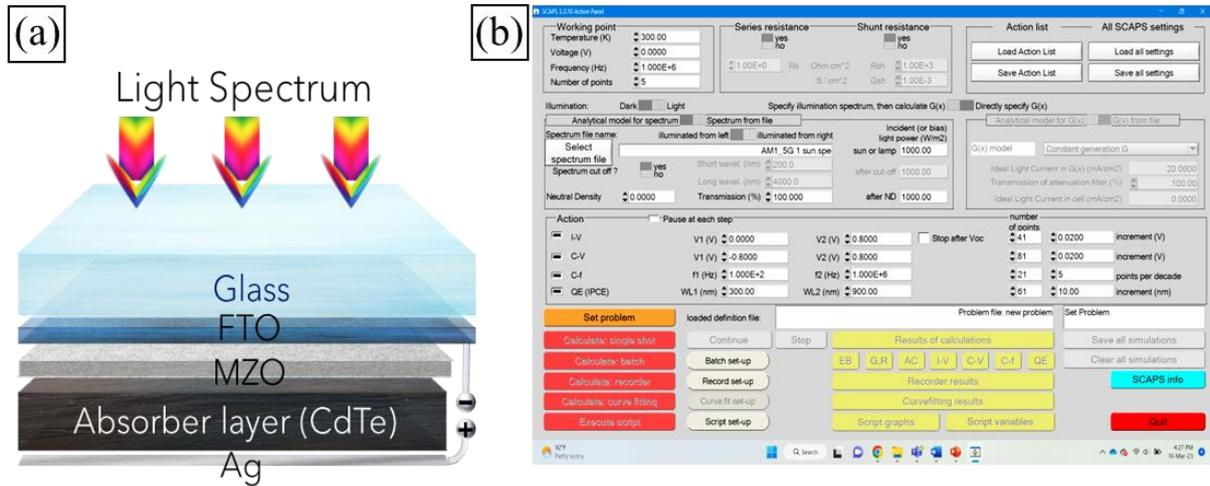


**Figure 1.** (**a**) CdTe device structure and (**b**) SCAPS simulation startup panel.
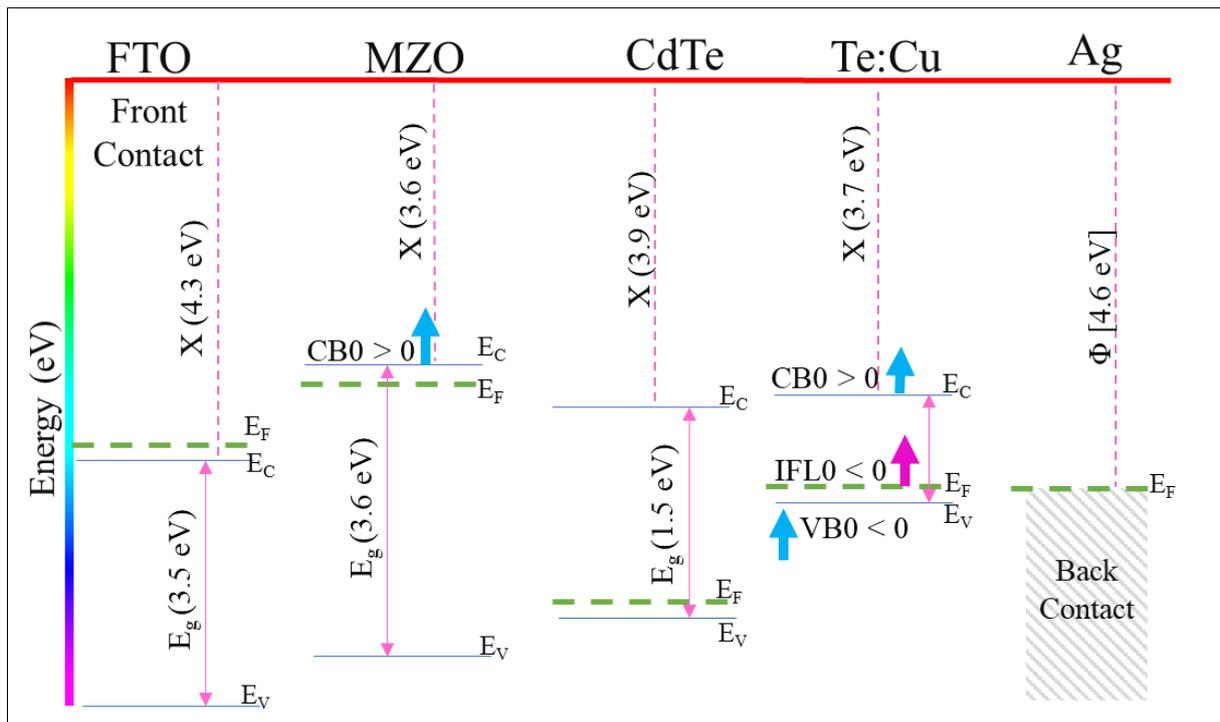


**Figure 2.** Energy band alignments of the non-interacting layers in CdTe thin film.

The Poisson's continuity equation is a primary equation used in this modeling to elucidate the significance of electrostatic charge potential and to determine the conservation of the carrier transport performance in the device [39], as given as in Equation (1):

$$\frac{\partial}{\partial x}\left(\varepsilon_o \varepsilon \frac{\partial \psi}{\partial x}\right) = -q\left(p - n + N_D^+ - N_A^- + \frac{\rho_{def}}{q}\right) \tag{1}$$

where $\varepsilon_o$ is the vacuum permittivity; $\varepsilon$ is the absolute permittivity; $\psi$ is the electrostatic potential; $q$ is the elementary charge; $N_D$ and $N_A$ are the donor and the acceptor concentration

respectively; and $\rho_{def}$ is the density defect. From this equation, the simulation analysis can distinguish the current–voltage characteristics based on the proposed structure and defined parameters. Moreover, the bias *QE* is an efficient method for qualitatively evaluating the built-in potential strength and back barrier heights [40], as shown in Equation (2):

$$QE\,(V) = QE_0 \left(1 + \frac{qJ_FR_S}{nKT}\right)^{-1} \tag{2}$$

where $J_F$, *Rs*, and *n* stand for forward current, shunt resistance, and diode quality factor. Ultimately, SCAPS was used in this research to assess the role of device performance after $CuCl_2$ doping and to improve the absorber's essential criteria for optimal device development, rather than relying entirely on complex experimental procedures.

## 3. Results and Discussion

Cu doping into the back-contact by $CuCl_2$ treatment approach is a common method to grow a p+ buffer between the p−CdTe and the metal electrode, as well as increasing carrier transport at the rear surface, resulting in the formation of an ohmic contact in CdTe thin films [41]. Excessive Cu+ diffusion into p-n junctions along grain boundaries, as well as the rapid formation of recombination centers, leads to shorter carrier lifetimes and low stability, making Cu-base back contact generation highly complex [42]. Thereby, the band energy of the generated buffer, doping concentration, and CdTe layer thickness are the most significant aspects in preventing Cu+ over diffusion into the bulk of the p-n junction [43]. The band-alignment plot shown in Figure 2 was based on charge-neutrality levels to establish a general scheme of energy-band alignments for materials with strong chemical bonds such as oxides and compound semiconductors in line with previous studies [44]. In the case of non-interacting thin film layers, the energy-band alignment at the interfaces can be described using the Schottky–Mott (SM) model in SCAPS, which assumes that the layers are separated by a thin insulating layer [45]. According to this model, the Fermi level of each layer will adjust to maintain charge neutrality, and the resulting band alignment will depend on the relative work functions of the two materials presented in Section 3.1. Moreover, when materials are exposed to ionizing radiations, they can undergo partial aging due to the formation of point defects, which alter the material's electrical characteristics, particularly the Eg [46]. Reasonable neutral interface defects are defined, and the Shockley–Read–Hall (SRH) model is used to calculate recombination currents for bulk defects. Moreover, accuracy in band alignment is achieved in this study by defining experimental data as thin film properties in SCAPS. Herein, the significance of the defined 2 nm [47] Te:Cu surface's band energy upon overall device performance is explored, followed by the evaluation of essential attributes for the development of Cu- back-contact-based CdTe device.

### 3.1. Effect of Te:Cu Band Offset on the Performance of CdTe Thin Films

Primarily, the energy band variation is performed within the experimentally observed $Cu_2Te$ bandgaps ranging from 0.5 to 1.8 eV [48,49], which are close to the bandgaps of $Sn_6Sb_{10}S_{21}$ thin films (Eg~1.67–1.68 eV) [50] and lower than those of $Ce_xCd_{1-x}S$ (Eg~2.24–2.40 eV) [51] and Sb-doped $Sn_3O_4$ (Eg~2.15–2.84 eV) [52]. Thus, the optimum bang gap of $Cu_2Te$ can be established for the effective performance of the rare Te:Cu buffer in CdTe. The line graph for Voc and Jsc-$_{JV}$ as a function of VBO and CBO at the CdTe/Te:Cu back buffer interface is shown in Figure 3. The energy band at the p-n junction is altered by the proposed band bending at the CdTe/Te:Cu back contact, which is also reported in other reports [53].

The band bending takes the shape of a desired +0.2 to +0.3 eV spike with rising band energy from all variants, whereas the VBO varies widely. The maximal value of the hole transport barrier (VBO) is at relatively low bandgaps ($\leq$0.7 eV) and when the energy band exceeds the CdTe absorbers band ($\geq$1.7 eV). Moreover, Figure 4 depicts the relative device performance when the width of the Te:Cu energy bands is varied. Regardless of the value of the CBO, the VOC rises, as plotted in Figure 4b, at a stoichiometric ratio as the VBO

becomes less negative, until it reaches a value of roughly $-0.1$ eV. The optimal bandgap range is demonstrated to be 1.1 eV $\leq$ Eg$_{Te:Cu}$ $\leq$ 1.3 eV, as validated by Figure 4b, where the maximum power point is obtained from the back buffer with the indicated band range.
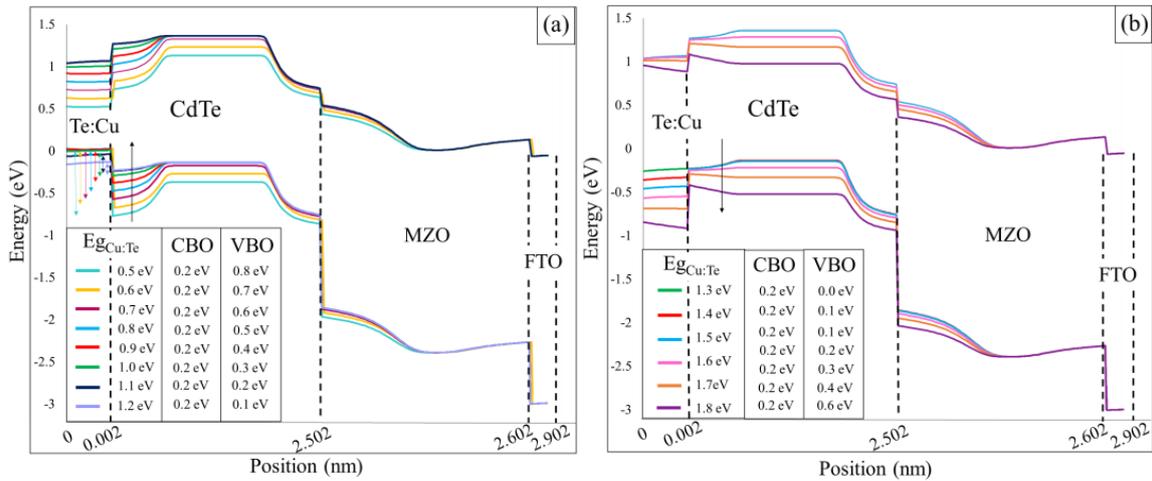


**Figure 3.** Band diagram of the proposed CdTe thin films with (**a**) $0.5 \leq$ Eg$_{Te:Cu}$ $\leq 1.2$ eV and (**b**) $1.3 \leq$ Eg$_{Te:Cu}$ $\leq 1.8$ eV.
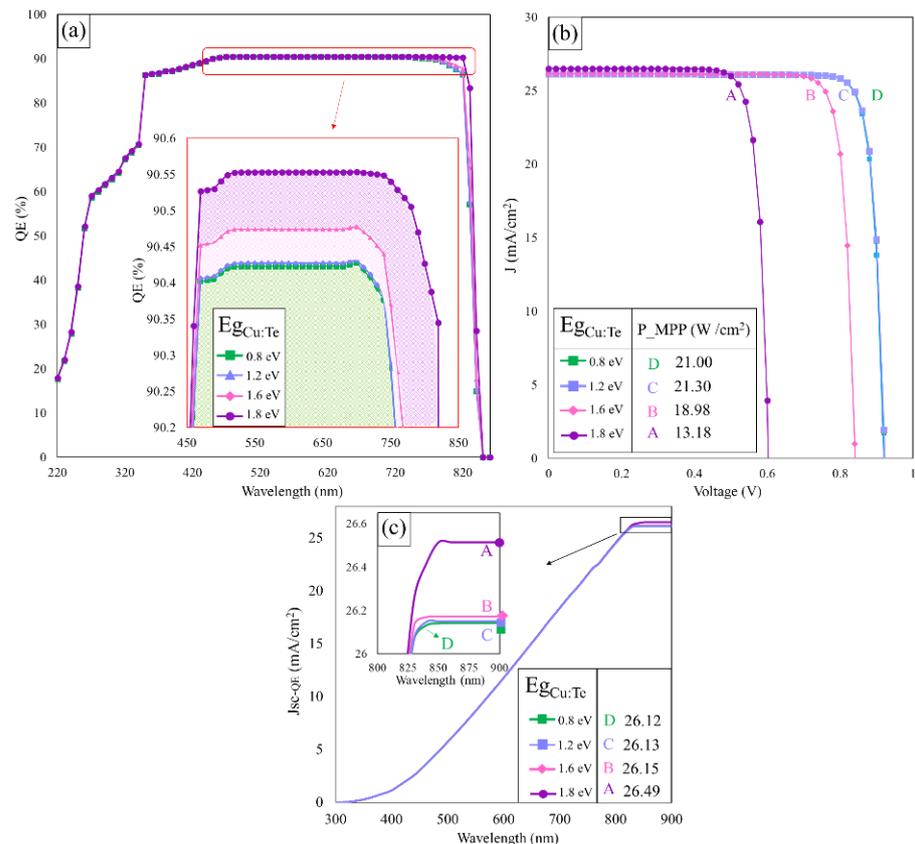


**Figure 4.** (**a**) QE spectra, (**b**) J-V curves, and (**c**) integrated photocurrent density of proposed CdTe thin films with varying Te:Cu bandgap.

The conduction and valence bands of the CdTe bend upward, toward the interface, by defining the IFL of the Te:Cu back buffer below that of the CdTe. This action repels electrons and limits interfacial recombination, allowing the over 20% efficiency to be achieved [54]. Figure 4c demonstrates the integrated photocurrent density and decreased recombination

rate for samples with Eg < 1.6 and better device performance, highlighting the crucial function of the BSF layer [55]. Performance parameters calculated by SCAPS upon varying the $Eg_{Te:Cu}$ are presented in Table 2. The energy band's performance characteristics are shown here to emphasize the changes in device performance caused by excessive Cu doping at the BSF layer, loss in fill factor (FF) in direct proportion to the Voc, reduction in the efficiency for Eg > 1.2 eV, and quick drop for Eg > 1.6 eV.

**Table 2.** Photoconductivity parameters of CdTe device for the BSF's band-energy variation.

| Parameters | Device | A ($Eg_{Cu:Te}$ = 0.8 eV) | B ($Eg_{Cu:Te}$ = 1.2 eV) | C ($Eg_{Cu:Te}$ = 1.6 eV) | D ($Eg_{Cu:Te}$ = 1.8 eV) |
|---|---|---|---|---|---|
| Voc (V) | | 0.92 | 0.92 | 0.84 | 0.60 |
| Jsc-$_{JV}$ (mA/cm$^2$) | | 26.14 | 26.15 | 26.17 | 26.51 |
| FF (%) | | 87.09 | 87.30 | 86.41 | 82.77 |
| Eta (%) | | 20.94 | 21.04 | 19.00 | 13.25 |
| V_MPP (V) | | 0.83 | 0.83 | 0.75 | 0.52 |
| J_MPP (mA/cm$^2$) | | 25.31 | 25.34 | 25.31 | 25.35 |

Furthermore, an ongoing detailed study on the ideal quantity of Cu dopant has revealed that the lower device efficiency with the reduction in the amount of Cu is primarily due to the insufficient ohmicity and hole concentration of the CdTe layer itself rather than an insufficient dopant ratio [56]. Thus, controlling the CdTe absorber thickness and its related band-bending limit allows the back surface to become less susceptible to recombination states [57]. In addition, the thickness of absorber layer is the key point for the absorption of a longer wavelength. When the absorber layer thickness increases, the light absorption of the longer wavelength also increases, which enhances the electron–hole pair generation and the performance of the CdTe solar cell [58]. Hence, the following analyses are all initiated respective to the optimal range of carrier density in CdTe layer. The variation of the CdTe layer thickness from 0.5 to 5 μm is presented in Figure 5a–d in terms of Voc, Jsc-$_{JV}$, FF, and η. Interestingly, the CdTe thickness seems unlikely to give significant impact to Voc from $10^{13}$ cm$^{-3}$ to $10^{18}$ cm$^{-3}$. However, the Voc increased after the carrier concentration increased to more than $10^{16}$ cm$^{-3}$. However, this is an expected result because a very high acceptor's carrier concentration tends to lead to a higher Voc since it happens to boost the built-in-potential in CdTe-absorber-layer region [59]. Thus, the carrier collection is much improved, and the space-charge region (SCR) is reduced [60]. Moreover, in Figure 5b, the variations of current density, Jsc-$_{JV}$, are evaluated. It shows the significant role that the CdTe absorber layer's thickness plays, as well as the acceptor carrier concentration. The Jsc-$_{JV}$ values increase when the CdTe absorber layer's thickness increases. As expected, the Jsc-$_{JV}$ gradually declines when the acceptor-carrier concentration increases. Between a thickness of 0.5 μm and 2.5 μm, the Jsc-$_{JV}$ value is at its lowest. Furthermore, higher hole densities in the absorber form a compact space charge area and stronger band bending near the Te:Cu layer [56].

When the absorber layer's thickness increased to higher than 2.5 μm, the Jsc-$_{JV}$ showed a slight increase toward 27 mA/cm$^2$. Subsequently, even with a higher acceptor concentration, when the CdTe absorber layer reaches around 4.0 μm, the Jsc-$_{JV}$ remains almost unchanged around 26.8 mA/cm$^2$, thus following the IFLO > 0 theory [28]. The fill factor (FF) of the CdTe solar cell performance is presented in Figure 5c. In general, the rudimental observation from the plot displays similar traits to the Voc contour plot in Figure 5a. Hence, the fill factor of solar cell devices correlates with the Voc values. While the CdTe absorber layer thickness increases, the FF also slightly increases when the acceptor-carrier concentration increases. It can be seen from Figure 5c that, when the carrier concentration exceeded around $10^{16}$ cm$^{-3}$, the FF was around 86% and 83% for CdTe thickness 2.5 μm and 5.0 μm, respectively, thus confirming the direct effect of CdTe carrier concentration on the Voc and FF changes. Lastly, Figure 5d illustrates that the conversion efficiency, η, increases when

the acceptor-carrier concentration, along with CdTe absorber layer's thickness, increases. Here, the efficiency is presented to be directly correlated to the Voc and FF values. Hence, when the carrier concentration exceeds $10^{16}$ cm$^{-3}$, regardless of thickness, the efficiency increases to more than 18%. Overall, for the minimum carrier concentration of $10^{16}$ cm$^{-3}$ and minimum thickness of 2.5 μm are shown to be crucial to achieve high efficiency and improved current in the Cu- back-contact-based CdTe device.
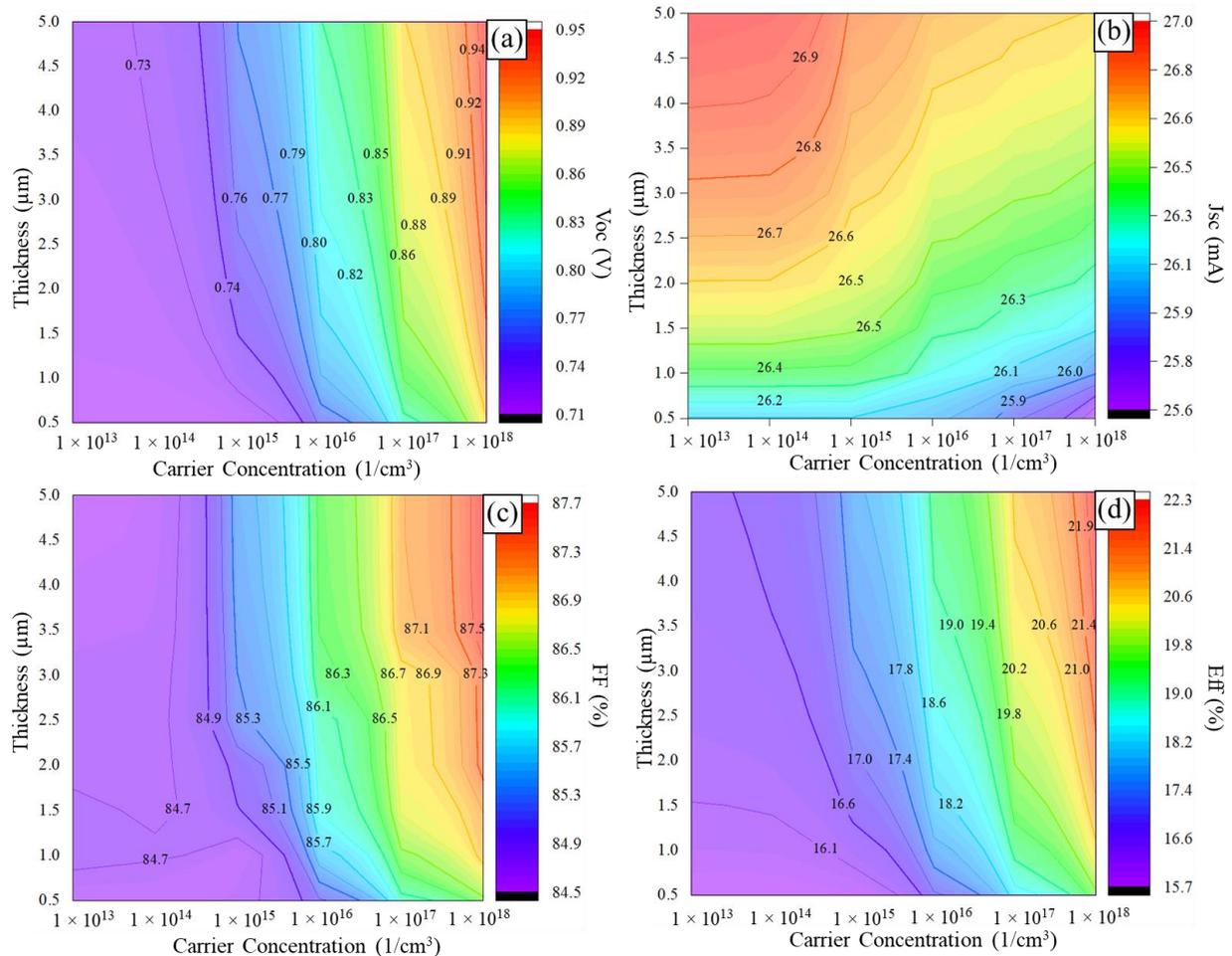


**Figure 5.** Contour plot of (**a**) Voc, (**b**) Jsc-$_{JV}$, (**c**) fill factor, and (**d**) efficiency with CdTe-layer-thickness and acceptor-concentration variation.

*3.2. Spectral Response Analysis*

The spectral response or the ratio of the current generated by the solar cell to the incident energy of sunlight is similar to quantum efficiency. When the number of photons incident on the solar cell is compared to the number of output electrons of the solar cell, it determines the quantum efficiency. When exposed to light, the generation of extra electron–hole pairs increases the drift current, decreasing the build-up potential at the junction and increasing Cu diffusion toward the junction [19]. In contrast, in a short-circuit scenario, the photogenerated current travels through the device, presumably recombining electrons and holes. Furthermore, it is reasonable to picture an electron flow coming from the back contact, which opposes the ionic form of Cu atoms and explains why, as previously said, the degradation effects are greater under open-circuit conditions in Cu-doped samples. Thus, by plotting the CdTe devices' external quantum efficiency (EQE), the useful wavelength range of the CdTe solar cell can be observed. Figure 6 illustrates the spectral response of the SCAPS modeling analysis on the Cu-dopped CdTe solar cell with respect to acceptor-carrier concentrations.
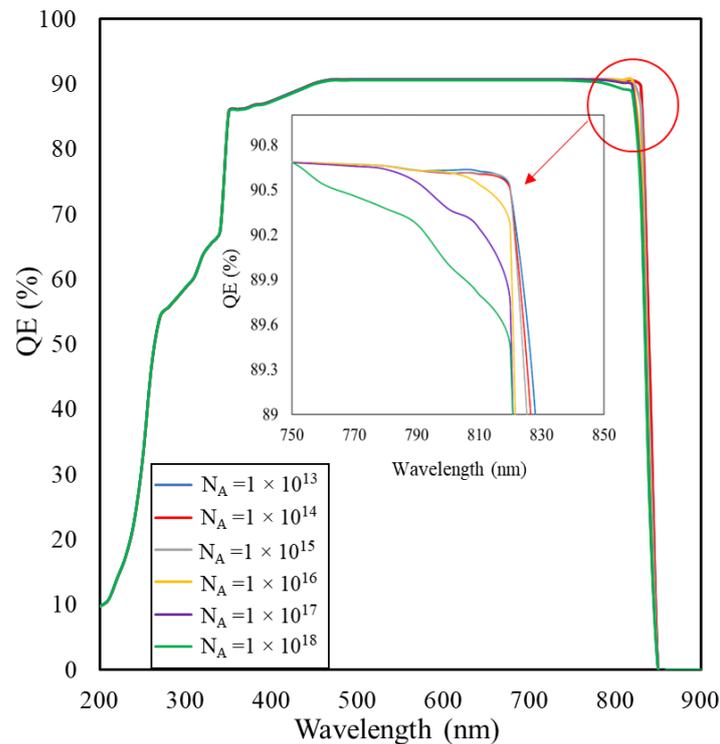
**Figure 6.** Effect of acceptor-carrier concentration on the CdTe solar cell's spectral response.

The parameters such as CdTe absorber layer thickness and CdTe bandgap are fixed at 2.5 μm and 1.50 eV, respectively. For the EQE response, the wavelength range extends from 200 nm to 900 nm. For all acceptor concentrations ($N_A$) of CdTe thin films, as simulated by SCAPS, the EQE shows a reducing pattern plot for the wavelengths close to the 800 nm. It corresponds to identical pattern for CdTe optical absorption that can determine the bandgap. The observations also agree with the results reported earlier [61]. The maximum absorption occurs in the range between 400 nm and 830 nm, where the average EQE is at least 80% with a maximum of 90% for CdTe with $N_A$:$10^{13}$ cm$^{-3}$. However, a CdTe with $N_A$:$10^{18}$ cm$^{-3}$ obtained 90% absorption for the wavelength range from 600 nm to 900 nm. It is worth mentioning that the SCAPS results described here correspond to numerical modeling, including the parameters of other thin films' layers, such as MZO and ITO. Since CdTe solar cell is a heterojunction, absorption from other layers within the visible-light range with defect parameters significantly tends to affect the spectral response analysis in the simulation [62]. Moreover, a higher acceptor concentration in the order of $10^{16}$ cm$^{-3}$ to $10^{18}$ cm$^{-3}$ tends to limit the space charge region's width, leading to the decrease of photon collection, as well as defects acting as recombination centers [63]. From the simulated EQE, it is also observed that higher acceptor concentration leads to Jsc-$_{JV}$ loss, primarily due to loss of long-wavelength photo-generated carriers. Theoretically, when the acceptor-carrier density in the absorber layer is comparable to the donor-carrier density in the buffer layer and the space charge region (SCR) is narrow, a huge number of photo-generated carriers with a short lifetime will recombine even at the back surface region, where there is no built-in electric field to assist carriers' collection [59]. Consequently, an acceptor concentration over $10^{16}$ cm$^{-3}$ with longer lifetime carriers is vital for the CdTe thin-film solar cell's performance.

### 3.3. Effect of Acceptor Concentration and Operational Temperature of CdTe Solar Cell

The working or operating temperature of a solar cell plays a significant role in evaluating its performance and stability. Figure 7a–d illustrate the effect on CdTe devices as a function of the carrier concentration on the operating temperature. The operating temperature varies from 300 K to 400 K in the SCAPS parameter. The Voc in Figure 7a

displays a detrimental effect when the temperature exceeds more than 360 K, for which the output voltage started from 0.4 V for an acceptor concentration of $10^{13}$ cm$^{-3}$. However, the Voc exhibits an increasing trend when the acceptor concentration rises from $10^{13}$ cm$^{-3}$ to $10^{18}$ cm$^{-3}$.
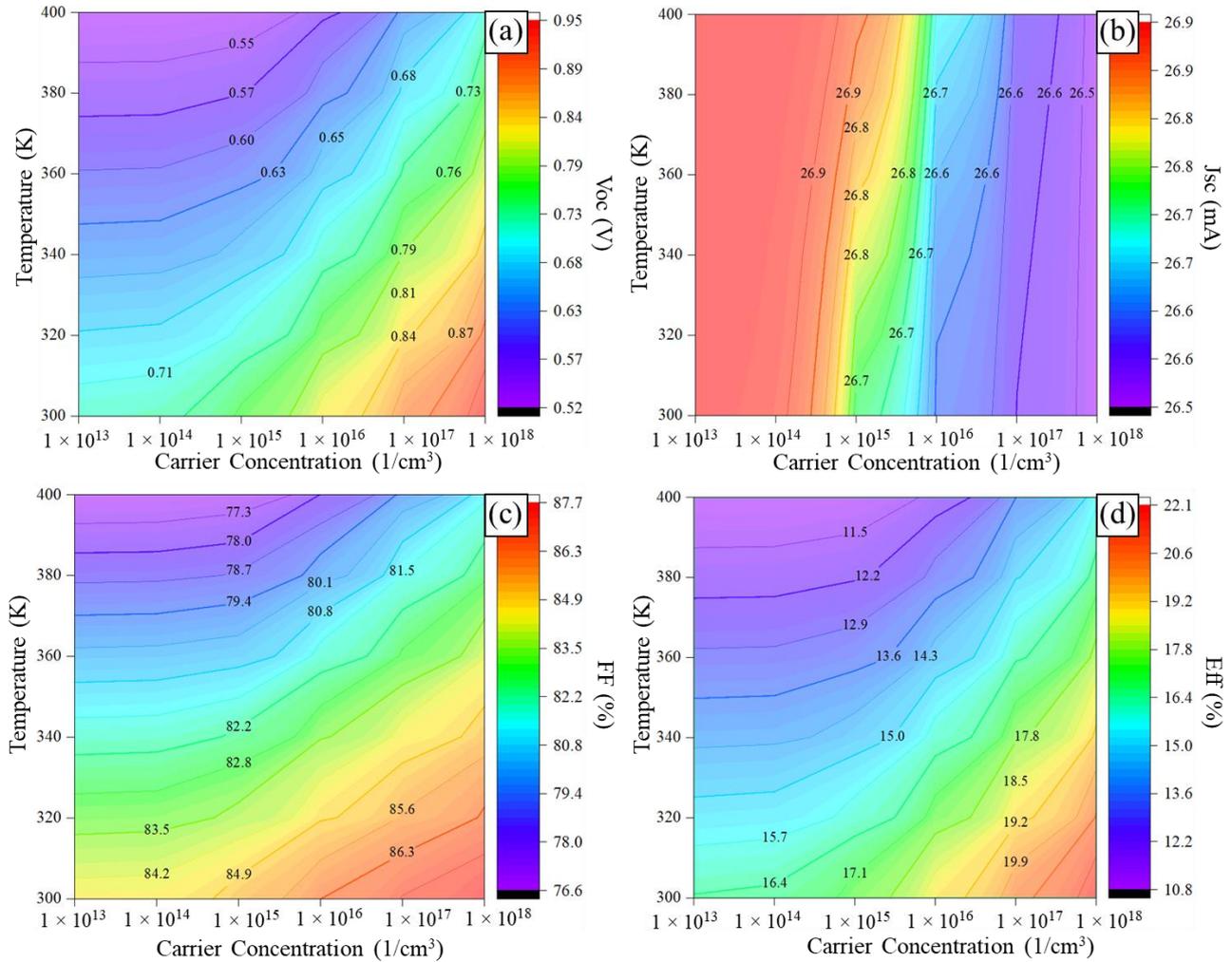


**Figure 7.** Contour plots of (**a**) Voc, (**b**) Jsc-JV, (**c**) FF, and (**d**) efficiency as the function of concentration and operational temperature of the CdTe solar cell.

When the operating temperature exceeds more than 340 K, the Voc decreases in response to the bandgap energy (Eg) increase for both the CdS layer and CdTe layer that is indirectly correlated to the Voc, as reported in [64]. Thus, as can be observed in Figure 7b, the current density, Jsc-JV, does not show any significant change when the temperature increases. It can be seen that the Jsc-JV decreases when the acceptor concentration increases. This is an expected result, as the Jsc-JV value is totally dependent on the spectral irradiance, as reported theoretically in details by Passler [65]. The Jsc-JV values remain constant, corresponding to the acceptor concentration and operating temperature. For an acceptor concentration close to $10^{15}$ cm$^{-3}$, the Jsc-JV value is approximately 25.5 mA for all operating temperatures. Figure 7c shows that the fill factor, FF, decreases when the temperature increases. However, when the acceptor concentration increases, the FF gradually rises, as well. For an operating temperature of 300 K and an acceptor concentration of $10^{13}$ cm$^{-3}$, the FF value is 76% and gradually increases to 86% from a $10^{15}$ cm$^{-3}$ acceptor concentration. Meanwhile, 400 K as the operating temperature of CdTe solar cell would limit the FF around 86% as the acceptor concentration reaches $10^{18}$ cm$^{-3}$. A similar trend for Voc was observed for the SCAPS output obtained from the theoretical values that suggests that the

FF values are directly correlated to Voc output. Nonetheless, the operating temperature in CdTe thin-film solar cell does not contribute much to calculated FF values, as it is mainly controlled by the Voc parameters, as discussed in [66]. In Figure 7d, the efficiency, η, reveals that the operating temperature has a substantial effect in the stability of the solar cell's performances. It is noteworthy to mention that the acceptor concentration also significantly contributes to the CdTe efficiency, as well. For an operating temperature of 300 K and acceptor concentration of around $10^{13}$ cm$^{-3}$, the CdTe solar cell's efficiency reaches between 10% and 12%. However, for the maximum operating temperature of 400 K, the efficiency of CdTe solar cell reaches between 8% and 11% for the similar acceptor concentration. When the maximum acceptor concentration of around $10^{18}$ cm$^{-3}$ is achieved, more than 20% efficiency is observed for a CdTe cell operating temperature between 300 K and 340 K. Hence, an operating temperature of more than 360 K limits the increase of efficiency below 20% even for the ideal case of $10^{18}$ cm$^{-3}$ of acceptor concentration in this simulation. The working or operating temperature is highly correlated to the optical characteristics and is able to change the bandgap of the materials, especially causing the CdTe layer to shift toward a higher bandgap [64]. This understanding was developed through the relative calculations among the efficiency, temperature, and acceptor-carrier concentration.

### 3.4. Effect of CdTe Bandgap Energy and Acceptor Concentration

One of the most important aspects for achieving higher performances and stability in a CdTe device is the optical bandgap energy. For the CdTe thin-film solar cell, the optimum bandgap is 1.50 eV. Figure 8a–d explains the simulation output for the CdTe device as a function of the bandgap and the acceptor concentration. The results obtained are Voc, Jsc-JV, FF, and efficiency for Figure 8a–d, respectively.
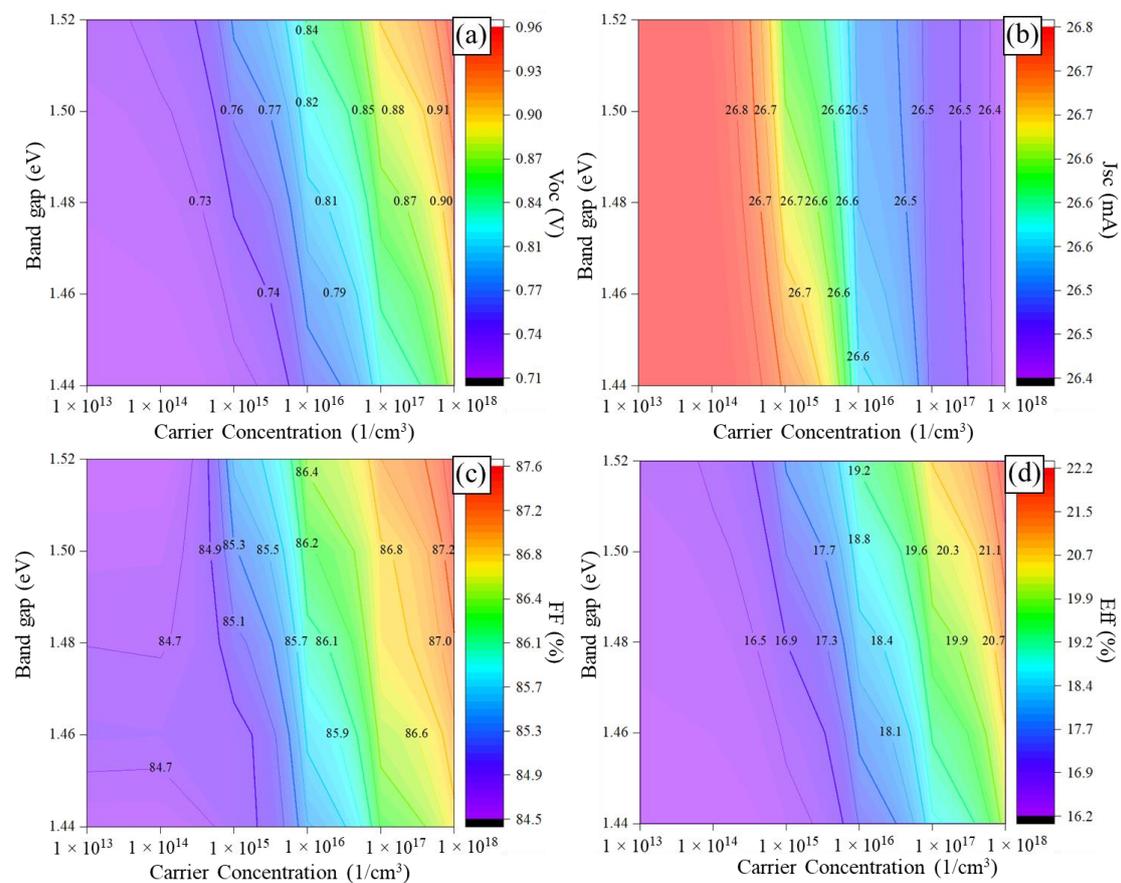


**Figure 8.** Contour plots of (**a**) Voc, (**b**) Jsc-JV, (**c**) FF, and (**d**) efficiency as the function of CdTe bandgap energy and acceptor concentration.

Interestingly, the simulation results for all parameters' output reveal that the carrier concentration in the Cu-doped CdTe absorber is the most effective factor to contribute to the CdTe device's performance. In Figure 8d, the efficiency increases by over 20% only with the carrier concentration of $10^{17}$ cm$^{-3}$ and above for a CdTe bandgap of >1.48 eV, whereas it continuously rises up around 21% of efficiency when the CdTe bandgap reaches 1.50 eV. As demonstrated here, bandgap energy is highly correlated with carrier density, as it controls the photo-generated carriers through absorption by photon excitation between the conduction band (CB) and valence band (VB) [67]. The stability of the CdTe solar cells' performance by this simulation is established through the CdTe absorber's bandgap optimization. Theoretically, when the solar cell is illuminated, absorption happens, followed by generation of electron–hole pairs as the inception of the carrier generation process, and affects the conductivity [68]. Thus, the output parameters change as the acceptor concentration increases from $10^{13}$ cm$^{-3}$ to $10^{18}$ cm$^{-3}$.

## 4. Conclusions

The inclusion of CuCl$_2$ treatment and the development of Cu$_2$Te buffer layers were examined through the changes brought in device-performance variables. The links between the back-contact characteristics, absorber thickness, doping density, and operating temperature with energy band offset transitions were also explored. The setting IFLO < 0, which counteracts with the electrons and reduces the interface states, enabled improved efficiency in Cu-doped back-contact-based models. Changes in the conversion efficiency with operating temperature and acceptor doping level considerably impacted the stability of the solar-cell performances. This correlation suggests that temperature has an influence on optical characteristics, and a temperature over 60 °C can cause detrimental effects via the CdTe bandgap expansion. With 25 °C as the operating temperature and around $10^{13}$ cm$^{-3}$ of acceptor concentration, the CdTe solar cell's efficiency decreased to about 11%. The efficiency of the CdTe solar cell further decreased to 8% for a 400 K operating temperature. In addition, changes in the CdTe acceptor concentration led to the spectral response change, especially in the longer wavelength region. However, the bandgap energy obtained from the simulation results did not show any effect on the device's performance characteristics. All in all, the incorporation of the Cu$_2$Te back layer with an optimized Eg$_{\text{Te:Cu}}$ = 1.2 eV resulted in the output parameters of Voc = 0.92 V, Jsc = 26.15 mA/cm$^2$, FF = 87.3%, and conversion efficiency of 21.04% as the best case here. A future study can center on the incorporation of novel materials with superior characteristics, as well as the optimization of experimental parameters in BSF and contact development for an improved Voc and increased carrier concentration rate. There is still a need to investigate BSF characteristics and how they impact defects, grain boundaries, carrier recombination, and mechanisms involved in CdTe devices. Finally, the contact formation and stability over time, as well as the scalability and repeatability of these procedures for the large-scale manufacture of CdTe solar cells, can be investigated.

**Author Contributions:** Conceptualization, M.N.H. and C.D.; data curation, M.N.H., C.D., A.N., H.N.R. and N.I.A.; formal analysis, M.N.H., C.D. and A.N.; funding acquisition, N.A.; investigation, M.N.H., A.N. and M.I.; methodology, C.D. and M.I.; project administration, M.I. and N.A.; resources, N.A.; software, M.N.H. and H.N.R.; validation, H.N.R.; visualization, A.N.; writing—original draft, C.D.; writing—review and editing, H.N.R., N.I.A. and N.A. All authors have read and agreed to the published version of the manuscript.

**Institutional Review Board Statement:** Not applicable.

**Informed Consent Statement:** Not applicable.

**Data Availability Statement:** Not applicable.

**Conflicts of Interest:** The authors declare no conflict of interest.

## References

1. Green, M.; Dunlop, E.; Hohl-Ebinger, J.; Yoshita, M.; Kopidakis, N.; Hao, X. Solar cell efficiency tables (version 57). *Prog. Photovolt. Res. Appl.* **2021**, *29*, 3–15. [CrossRef]
2. Benick, J.; Richter, A.; Müller, R.; Hauser, H.; Feldmann, F.; Krenckel, P.; Riepe, S.; Schindler, F.; Schubert, M.C.; Hermle, M. High-efficiency n-type HP mc silicon solar cells. *IEEE J. Photovolt.* **2017**, *7*, 1171–1175. [CrossRef]
3. Kovachov, S.; Bohdanov, I.; Karipbayev, Z.; Suchikova, Y.; Tsebriienko, T.; Popov, A.I. Layer-by-Layer Synthesis and Analysis of the the Phase Composition of $Cd_xTe_yO_z$/CdS/por-ZnO/ZnO Heterostructure. In Proceedings of the 2022 IEEE 3rd KhPI Week on Advanced Technology (KhPIWeek), Kharkiv, Ukraine, 3–7 October 2022; pp. 1–6.
4. Heredia-Cancino, J.; Mendoza-Peña, K.; Higuera-Valenzuela, H.; Soto B., M.A.; Ochoa-Landín, R.; Castillo, S.J. Synthesis Optimization of Cadmium Carbonate Films as Potential Precursor to Produce CdSe, CdTe, and CdO Films. *Coatings* **2022**, *12*, 1691. [CrossRef]
5. Balakhayeva, R.; Akilbekov, A.; Baimukhanov, Z.; Giniyatova, S.; Zdorovets, M.; Gorin, Y.; Popov, A.; Dauletbekova, A.J.S.; Technology, C. Structure properties of CdTe nanocrystals created in $SiO_2$/Si ion track templates. *Surf. Coat. Technol.* **2020**, *401*, 126269. [CrossRef]
6. Fiducia, T.; Howkins, A.; Abbas, A.; Mendis, B.; Munshi, A.; Barth, K.; Sampath, W.; Walls, J. Selenium passivates grain boundaries in alloyed CdTe solar cells. *Sol. Energy Mater. Sol. Cells* **2022**, *238*, 111595. [CrossRef]
7. Seck, S.M.; Ndiaye, E.N.; Fall, M.; Charvet, S. Study of Efficiencies CdTe/CdS Photovoltaic Solar Cell According to Electrical Properties by Scaps Simulation. *Nat. Resour.* **2020**, *11*, 147–155. [CrossRef]
8. Ščajev, P.; Miasojedovas, S.; Mekys, A.; Kuciauskas, D.; Lynn, K.G.; Swain, S.K.; Jarašiūnas, K. Excitation-dependent carrier lifetime and diffusion length in bulk CdTe determined by time-resolved optical pump-probe techniques. *J. Appl. Phys.* **2018**, *123*, 025704. [CrossRef]
9. Houshmand, M.; Zandi, M.H.; Gorji, N.E. SCAPS modeling for degradation of ultrathin CdTe Films: Materials interdiffusion. *JOM* **2015**, *67*, 2062–2070. [CrossRef]
10. Fang, Z.; Wang, X.C.; Wu, H.C.; Zhao, C.Z. Achievements and challenges of CdS/CdTe solar cells. *Int. J. Photoenergy* **2011**, *2011*, 297350. [CrossRef]
11. Siepchen, B.; Späth, B.; Drost, C.; Krishnakumar, V.; Kraft, C.; Winkler, M.; König, J.; Bartholomé, K.; Peng, S. A Simple Sb 2 Te 3 Back-Contact Process for CdTe Solar Cells. *J. Electron. Mater.* **2015**, *44*, 3354–3359. [CrossRef]
12. Yang, R.; Wang, D.; Jeng, M.; Ho, K.; Wang, D. Stable CdTe thin film solar cells with a MoOx back-contact buffer layer. *Prog. Photovolt. Res. Appl.* **2016**, *24*, 59–65. [CrossRef]
13. Zhang, M.-J.; Lin, Q.; Yang, X.; Mei, Z.; Liang, J.; Lin, Y.; Pan, F. Novel p-type conductive semiconductor nanocrystalline film as the back electrode for high-performance thin film solar cells. *Nano Lett.* **2016**, *16*, 1218–1223. [CrossRef] [PubMed]
14. Weng, Z.; Ma, S.; Zhu, H.; Ye, Z.; Shu, T.; Zhou, J.; Wu, X.; Wu, H. CdTe thin film solar cells with a SnTe buffer layer in back contact. *Sol. Energy Mater. Sol. Cells* **2018**, *179*, 276–282. [CrossRef]
15. Ferekides, C.; Balasubramanian, U.; Mamazza, R.; Viswanathan, V.; Zhao, H.; Morel, D. CdTe thin film solar cells: Device and technology issues. *Sol. Energy* **2004**, *77*, 823–830. [CrossRef]
16. Song, H.; Wu, X.; Zheng, J.; Yan, Q. Study of CuxTe polycrystalline thin films for CdTe solar cells. In Proceedings of the 2010 Asia-Pacific Power and Energy Engineering Conference, Chengdu, China, 28–31 March 2010; pp. 1–4.
17. Salmón-Gamboa, J.; Barajas-Aguilar, A.; Ruiz-Ortega, L.; Garay-Tapia, A.; Jiménez-Sandoval, S. Vibrational and electrical properties of $Cu_{2−x}Te$ films: Experimental data and first principle calculations. *Sci. Rep.* **2018**, *8*, 8093. [CrossRef]
18. Li, D.-B.; Bista, S.S.; Awni, R.A.; Subedi, K.K.; Shrestha, N.; Neupane, S.; Jamarkattel, M.K.; Song, Z.; Ellingson, R.J.; Yan, Y. Fabricating Efficient CdTe Solar Cells: The Effect of Cu Precursor. In Proceedings of the 2021 IEEE 48th Photovoltaic Specialists Conference (PVSC), Fort Lauderdale, FL, USA, 20–25 June 2021; pp. 2200–2203.
19. Gretener, C.; Perrenoud, J.; Kranz, L.; Cheah, E.; Dietrich, M.; Buecheler, S.; Tiwari, A. New perspective on the performance stability of CdTe solar cells. *Sol. Energy Mater. Sol. Cells* **2016**, *146*, 51–57. [CrossRef]
20. Perrenoud, J.; Kranz, L.; Gretener, C.; Pianezzi, F.; Nishiwaki, S.; Buecheler, S.; Tiwari, A. A comprehensive picture of Cu doping in CdTe solar cells. *J. Appl. Phys.* **2013**, *114*, 174505. [CrossRef]
21. Guo, D.; Fang, T.; Moore, A.; Brinkman, D.; Akis, R.; Krasikov, D.; Sankin, I.; Ringhofer, C.; Vasileska, D. Numerical simulation of copper migration in single crystal CdTe. *IEEE J. Photovolt.* **2016**, *6*, 1286–1291. [CrossRef]
22. Aris, K.A.; Rahman, K.S.; Enam, F.T.; Kamaruzzaman, M.I.B.; Yahya, I.B.; Amin, N. An investigation on copper doping to CdTe absorber layers in CdTe thin film solar cells. In Proceedings of the 2016 International Conference on Advances in Electrical, Electronic and Systems Engineering (ICAEES), Putrajaya, Malaysia, 14–16 November 2016; pp. 405–408.

23. Hadjab, M.; Wagner, J.-M.; Bouzid, F.; Boudour, S.; Hadj Larbi, A.; Bennacer, H.; Ziane, M.I.; Saeed, M.; Abid, H.; Berrah, S.; et al. A numerical optimization study of CdS and Mg0. 125Zn0. 875O buffer layers in CIGS-based solar cells using wx AMPS-1D package. *Int. J. Model. Simul.* **2022**, *42*, 179–191. [CrossRef]

24. Kowsar, A.; Billah, M.; Dey, S.; Debnath, S.C.; Yeakin, S.; Farhad, S.F.U. Comparative Study on Solar Cell Simulators. In Proceedings of the 2019 2nd International Conference on Innovation in Engineering and Technology (ICIET), Dhaka, Bangladesh, 23–24 December 2019; pp. 1–6.

25. Burgelman, M.; Nollet, P.; Degrave, S. Modelling polycrystalline semiconductor solar cells. *Thin Solid Film.* **2000**, *361*, 527–532. [CrossRef]

26. Kranz, L.; Gretener, C.; Perrenoud, J.; Schmitt, R.; Pianezzi, F.; La Mattina, F.; Blösch, P.; Cheah, E.; Chirilă, A.; Fella, C.M. Doping of polycrystalline CdTe for high-efficiency solar cells on flexible metal foil. *Nat. Commun.* **2013**, *4*, 2306. [CrossRef] [PubMed]

27. Bista, S.S.; Li, D.-B.; Awni, R.A.; Song, Z.; Subedi, K.K.; Shrestha, N.; Rijal, S.; Neupane, S.; Grice, C.R.; Phillips, A.B. Effects of Cu Precursor on the Performance of Efficient CdTe Solar Cells. *ACS Appl. Mater. Interfaces* **2021**, *13*, 38432–38440. [CrossRef] [PubMed]

28. Liyanage, G.K.; Phillips, A.B.; Alfadhili, F.K.; Ellingson, R.J.; Heben, M.J. The role of back buffer layers and absorber properties for >25% efficient CdTe solar cells. *ACS Appl. Energy Mater.* **2019**, *2*, 5419–5426. [CrossRef]

29. Teyou Ngoupo, A.; Ouédraogo, S.; Ndjaka, J.M. Numerical analysis of interface properties effects in CdTe/CdS: O thin film solar cell by SCAPS-1D. *Indian J. Phys.* **2019**, *93*, 869–881. [CrossRef]

30. Munshi, A.H.; Kephart, J.M.; Abbas, A.; Shimpi, T.M.; Barth, K.L.; Walls, J.M.; Sampath, W.S. Polycrystalline CdTe photovoltaics with efficiency over 18% through improved absorber passivation and current collection. *Sol. Energy Mater. Sol. Cells* **2018**, *176*, 9–18. [CrossRef]

31. Al-Luhaiby, A.K. Studying the effect of temperature and resistances of series (Rs) and parallel (Rsh) on the performance of the solar cell (FTO/Zn$_2$SnO$_4$/CdS: O/CdTe/Cu$_2$Te) using the SCAPS-1D program. *J. Educ. Sci.* **2022**, *31*, 49–66. [CrossRef]

32. Good, B.; Colegrove, E.; Reese, M.O.; Cells, S. Effects of absorber near-interface compensation on Cd (Se, Te) solar cell performance. *Sol. Energy Mater. Sol. Cells* **2022**, *246*, 111928. [CrossRef]

33. Zyoud, S.H.; Zyoud, A.H.; Ahmed, N.M.; Prasad, A.R.; Khan, S.N.; Abdelkader, A.F.; Shahwan, M. Numerical modeling of high conversion efficiency FTO/ZnO/CdS/CZTS/MO thin film-based solar cells: Using SCAPS-1D software. *Crystals* **2021**, *11*, 1468. [CrossRef]

34. Matin, M.; Tomal, M.; Robin, A. Copper telluride as a nobel BSF material for high performance ultra thin CdTe PV cell. In Proceedings of the 2013 International Conference on Informatics, Electronics and Vision (ICIEV), Dhaka, Bangladesh, 17–18 May 2013; pp. 1–5.

35. Guo, D.; Akis, R.; Brinkman, D.; Moore, A.; Fang, T.; Sankin, I.; Vasileska, D.; Ringhofer, C. Cu migration and its impact on the metastable behavior of CdTe solar cells. In Proceedings of the 2015 IEEE 42nd Photovoltaic Specialist Conference (PVSC), New Orleans, LA, USA, 14–19 June 2015; pp. 1–5.

36. Arellano-Tanori, O.; Acosta-Enríquez, M.; Ochoa-Landin, R.; Iniguez-Palomares, R.; Mendivil-Reynoso, T.; Flores-Acosta, M.; Castillo, S. Copper-selenide and copper-telluride composites powders sintetized by ionic exchange. *Chalcogenide Lett* **2014**, *11*, 13–19.

37. Hossain, M.; Rahman, K.; Islam, M.; Akhtaruzzaman, M.; Misran, H.; Alghoul, M.; Amin, N. Growth optimization of ZnxCd1-xS films on ITO and FTO coated glass for alternative buffer application in CdTe thin film solar cells. *Opt. Mater.* **2018**, *86*, 270–277. [CrossRef]

38. Hsiao, K.-J. Energy-band barrier to improve open-circuit voltage of CdTe solar cells. *Sol. Energy Mater. Sol. Cells* **2014**, *120*, 647–653. [CrossRef]

39. Gretener, C.; Perrenoud, J.; Kranz, L.; Kneer, L.; Schmitt, R.; Buecheler, S.; Tiwari, A.N. CdTe/CdS thin film solar cells grown in substrate configuration. *Prog. Photovolt. Res. Appl.* **2013**, *21*, 1580–1586. [CrossRef]

40. Wang, T.; Ren, S.; Li, C.; Li, W.; Liu, C.; Zhang, J.; Wu, L.; Li, B.; Zeng, G. Exploring window buffer layer technology to enhance CdTe solar cell performance. *Sol. Energy* **2018**, *164*, 180–186. [CrossRef]

41. Kim, S.; Jeon, J.; Suh, J.; Hong, J.; Kim, T.; Kim, K.; Cho, S. Comparative study of Cu$_2$Te and Cu back contact in CdS/CdTe solar cell. *J. Korean Phys. Soc.* **2018**, *72*, 780–785. [CrossRef]

42. Luo, G.; Yang, D.; Guo, X.; Yang, Y.; Luo, S.; Zhang, J.; Long, M.; Xiang, L.; Li, Q.; Wang, T. Quasi-ohmic contact formation assisted by the back contact with Cu2Te nanoparticles@ reduced graphene oxide composites for highly efficient CdTe solar cells. *J. Alloys Compd.* **2022**, *921*, 166100. [CrossRef]

43. Kuciauskas, D.; Dippo, P.; Kanevce, A.; Zhao, Z.; Cheng, L.; Los, A.; Gloeckler, M.; Metzger, W.K. The impact of Cu on recombination in high voltage CdTe solar cells. *Appl. Phys. Lett.* **2015**, *107*, 243906. [CrossRef]

44. Allam, Z.; Boudaoud, C.; Soufi, A.; Bouchachia, B. Performance Parameters of CdTe/CdS Solar Cell with Deferent Contact Schottky. In *Artificial Intelligence and Heuristics for Smart Energy Efficiency in Smart Cities: Case Study: Tipasa, Algeria*; Springer International Publishing: Berlin/Heidelberg, Germany, 2022; pp. 769–778.

45. Li, S.; Chen, F.; Schafranek, R.; Bayer, T.J.; Rachut, K.; Fuchs, A.; Siol, S.; Weidner, M.; Hohmann, M.; Pfeifer, V.J. Intrinsic energy band alignment of functional oxides. *Phys. Status Solidi (RRL) Rapid Res. Lett.* **2014**, *8*, 571–576. [CrossRef]

46. Dzade, N. First-principles insights into the electronic structure, optical and band alignment properties of earth-abundant Cu$_2$SrSnS$_4$ solar absorber. *Sci. Rep.* **2021**, *11*, 4755. [CrossRef]

47. Rimmaudo, I.; Salavei, A.; Rossi, F.; Buffagni, E.; Ferrari, C.; Giarola, M.; Mariotto, G.; Romeo, A. Study of the effect of absorber etching on the back contact performance of CdTe solar cells. In Proceedings of the 28th European Photovoltaic Solar Energy Conference and Exhibition, Paris, France, 30 September–4 October 2013; pp. 2389–2392.

48. Dobson, K.D.; Visoly-Fisher, I.; Hodes, G.; Cahen, D. Stability of CdTe/CdS thin-film solar cells. *Sol. Energy Mater. Sol. Cells* **2000**, *62*, 295–325. [CrossRef]

49. Sirusi, A.A.; Ballikaya, S.; Chen, J.-H.; Uher, C.; Ross Jr, J.H. Band Ordering and Dynamics of $Cu_{2−x}$ Te and Cu1. 98Ag0. 2Te. *J. Phys. Chem. C* **2016**, *120*, 14549–14555. [CrossRef]

50. Chongngam, P.; Tubtimtae, A. Structural, optical, and electrochemical characteristics of undoped and In3+-doped tin antimony sulfide thin films for device applications. *J. Mater. Sci. Mater. Electron.* **2023**, *34*, 71. [CrossRef]

51. Chiristina, E.N.; Rahayu, S.U.; Tubtimtae, A.; Shi, J.-B.; Lee, M.-W. Rare-earth-incorporated ternary $Ce_xCd_{1−x}S$ quantum dot-sensitized solar cells. *RSC Adv.* **2022**, *12*, 31093–31101. [CrossRef] [PubMed]

52. Suwannakham, N.; Tubtimtae, A.; Wongrat, E. Structural, linear/non-linear optical, optoelectrical, and electrical properties of novel crystalline antimony-doped tin oxide thin films synthesized by the chemical deposition method. *Phys. B Condens. Matter* **2023**, *649*, 414440. [CrossRef]

53. Li, J.V.; Halverson, A.F.; Sulima, O.V.; Bansal, S.; Burst, J.M.; Barnes, T.M.; Gessert, T.A.; Levi, D.H. Theoretical analysis of effects of deep level, back contact, and absorber thickness on capacitance–voltage profiling of CdTe thin-film solar cells. *Sol. Energy Mater. Sol. Cells* **2012**, *100*, 126–131. [CrossRef]

54. Alfadhili, F.K.; Phillips, A.B.; Liyanage, G.K.; Gibbs, J.M.; Jamarkattel, M.K.; Heben, M.J. Controlling band alignment at the back interface of cadmium telluride solar cells using ZnTe and Te buffer layers. *MRS Adv.* **2019**, *4*, 913–919. [CrossRef]

55. Hosen, A.; Al Ahmed, S.R. Performance analysis of SnS solar cell with a hole transport layer based on experimentally extracted device parameters. *J. Alloy. Compd.* **2022**, *909*, 164823. [CrossRef]

56. Artegiani, E.; Major, J.D.; Shiel, H.; Dhanak, V.; Ferrari, C.; Romeo, A. How the amount of copper influences the formation and stability of defects in CdTe solar cells. *Sol. Energy Mater. Soral Cells* **2020**, *204*, 110228. [CrossRef]

57. Ablekim, T.; Colegrove, E.; Metzger, W.K. Interface engineering for 25% CdTe solar cells. *ACS Appl. Energy Mater.* **2018**, *1*, 5135–5139. [CrossRef]

58. Kanevce, A.; Gessert, T.A. Optimizing CdTe solar cell performance: Impact of variations in minority-carrier lifetime and carrier density profile. *IEEE J. Photovolt.* **2011**, *1*, 99–103. [CrossRef]

59. Song, T.; Kanevce, A.; Sites, J.R. Emitter/absorber interface of CdTe solar cells. *J. Appl. Phys.* **2016**, *119*, 233104. [CrossRef]

60. Kanevce, A.; Reese, M.O.; Barnes, T.; Jensen, S.; Metzger, W. The roles of carrier concentration and interface, bulk, and grain-boundary recombination for 25% efficient CdTe solar cells. *J. Appl. Phys.* **2017**, *121*, 214506. [CrossRef]

61. Tinedert, I.; Pezzimenti, F.; Megherbi, M.; Saadoune, A. Design and simulation of a high efficiency CdS/CdTe solar cell. *Optik* **2020**, *208*, 164112. [CrossRef]

62. Treharne, R.; Seymour-Pierce, A.; Durose, K.; Hutchings, K.; Roncallo, S.; Lane, D. Optical design and fabrication of fully sputtered CdTe/CdS solar cells. In *Journal of Physics: Conference Series*; IOP Publishing: Bristol, UK, 2011; p. 012038.

63. Sameera, J.N.; Jhuma, F.A.; Rashid, M.J. Numerical approach to optimizing the doping concentration of the absorber layer to enhance the performance of a CdTe solar cell. *Semicond. Sci. Technol.* **2020**, *36*, 015022. [CrossRef]

64. Singh, P.; Ravindra, N.M. Temperature dependence of solar cell performance—An analysis. *Sol. Energy Mater. Sol. Cells* **2012**, *101*, 36–45. [CrossRef]

65. Pässler, R. Parameter sets due to fittings of the temperature dependencies of fundamental bandgaps in semiconductors. *Phys. Status Solidi (b)* **1999**, *216*, 975–1007. [CrossRef]

66. Singh, P.; Singh, S.; Lal, M.; Husain, M. Temperature dependence of I–V characteristics and performance parameters of silicon solar cell. *Sol. Energy Mater. Sol. Cells* **2008**, *92*, 1611–1616. [CrossRef]

67. Green, M.A. Solar cells: Operating principles, technology, and system applications. *Englewood Cliffs* **1982**, *1*, 274.

68. Sze, S.M.; Li, Y.; Ng, K.K. *Physics of Semiconductor Devices*; John Wiley & Sons: Hoboken, NJ, USA, 2021.